Macroscopically ordered state in an exciton system

L. V. Butov*†, A. C. Gossard‡ & D. S. Chemla*§

** Materials Sciences Division, E. O. Lawrence Berkeley National Laboratory;*
§ Department of Physics, University of California at Berkeley, Berkeley, California 94720, USA
† Institute of Solid State Physics, Russian Academy of Sciences, 142432 Chernogolovka, Russia
‡ Department of Electrical and Computer Engineering, University of California, Santa Barbara, California 93106, USA

There is a rich variety of quantum liquids—such as superconductors, liquid helium and atom Bose–Einstein condensates—that exhibit macroscopic coherence in the form of ordered arrays of vortices[1–4]. Experimental observation of a macroscopically ordered electronic state in semiconductors has, however, remained a challenging and relatively unexplored problem. A promising approach for the realization of such a state is to use excitons, bound pairs of electrons and holes that can form in semiconductor systems. At low densities, excitons are Bose-particles[5], and at low temperatures, of the order of a few kelvin, excitons can form a quantum liquid—that is, a statistically degenerate Bose gas or even a Bose–Einstein condensate[5–7]. Here we report photoluminescence measurements of a quasi-two-dimensional exciton gas in GaAs/AlGaAs coupled quantum wells and the observation of a macroscopically ordered exciton state. Our spatially resolved measurements reveal fragmentation of the ring-shaped emission pattern into circular structures that form periodic arrays over lengths up to 1 mm.

We studied spatially resolved photoluminescence (PL) of quasi-two-dimensional gases of indirect excitons in GaAs/AlGaAs coupled quantum wells (QWs); see Fig. 1b. Coupled QWs form a unique system where a cold exciton gas, and, more generally, a cold gas of light boson quasiparticles, can be created[8–12]. The indirect excitons in coupled QWs are characterized by high cooling rates, three orders of magnitude higher than in bulk GaAs, and a long lifetime, more than three orders of magnitude longer than in a single GaAs QW. This lifetime is much longer than the characteristic timescale for cooling of initially hot photogenerated excitons down to temperatures well below 1 K, where the dilute Bose gas of indirect excitons becomes statistically degenerate[10]. Because the exciton mass, M, is small, smaller than the free electron mass m_0, the quantum degeneracy temperature $T_0 = (\pi\hbar^2 n)/(2Mgk_B)$ (where g is the spin degeneracy of the exciton state, k_B is the Boltzmann constant and $\hbar$ is the Planck constant) exceeds 1 K at experimentally accessible exciton densities, n.

Another important advantage of the system is a repulsive interaction between the indirect excitons, characteristic of oriented dipoles: indirect excitons are dipoles oriented perpendicularly to the QW plane (Fig. 1b). The repulsive interaction stabilizes the exciton state against the formation of metallic electron–hole droplets[13,14], reinforces the Bose–Einstein condensation[15] and results in a screening of an in-plane random potential (which is caused by interface fluctuations, impurities, and so on, and is unavoidable in any QW sample). In two-dimensional systems with a repulsive interaction a phase transition to a superfluid exciton state is possible at finite temperatures[16]. The latter is characterized by a long-range order at low temperatures[17].

A high density of indirect excitons is achieved by nonresonant laser photoexcitation with energies at or above the direct exciton resonance where the photon absorption coefficient is high (Fig. 1b). In a quasiequilibrium, almost all photoexcited carriers relax to the indirect exciton states because they are lower in energy (the ratio

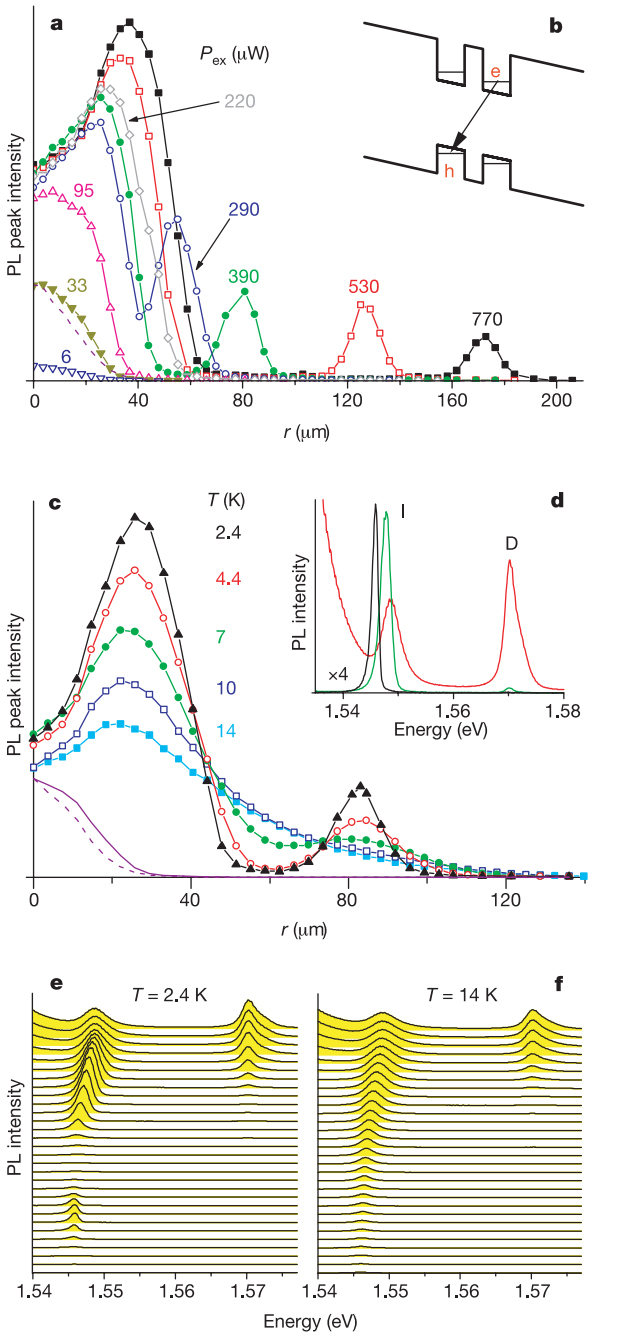

Figure 1 Radial dependence of the indirect exciton photoluminescence (PL). **a**, Peak intensity of the indirect exciton PL versus r, the distance from the excitation spot centre, at $T = 1.8$ K, gate voltage $V_g = 1.22$ V, and the excitation powers $P_{ex} = 6$, 33, 95, 220, 290, 390, 530 and 770 μW. **c**, Peak intensity of the indirect exciton PL versus r at $P_{ex} = 390$ μW, $V_g = 1.22$ V, and $T = 2.4$, 4.4, 7, 10 and 14 K. The excitation spot profiles are shown by the purple dashed lines in **a** and **c**. The solid purple line in **c** shows the peak intensity of the direct exciton PL. The corresponding spatial dependence of the PL spectra at $T = 2.4$ and 14 K are shown in **e** and **f**. The uppermost spectra are recorded at $r = 0$, the lowest at $r = 107$ μm, and the step is 3.7 μm. The indirect exciton PL line (I) is at about 1.545–1.55 eV; the direct PL line (D) is at about 1.57 eV; the broad line arising below the indirect exciton line is the bulk n^+-GaAs emission. The selected spectra at $T = 2.4$ K are shown in **d**: in the excitation spot centre at $r = 0$ (red), in the internal ring centre at $r = 29$ μm (green), and in the external ring centre at $r = 83$ μm (black, the intensity is multiplied by 4). **b**, Energy band diagram of the CQW structures; e, electron; h, hole. The PL of indirect excitons is characterized by the rings centred at the excitation spot: the internal ring is located near the edge of the excitation spot, while the external ring is observed far away from the excitation spot.

between the indirect and direct exciton densities is typically $>10^4$). The initially photogenerated excitons are hot, but quickly cool down to the lattice temperature, $T_{lattice}$, by phonon emission. For example, the exciton temperature, T_X, can drop down to 400 mK in about 5 ns, that is, a time much shorter than the indirect exciton lifetime[10]. Therefore, there are two ways to overcome the obstacle of hot generation and study cold gases of indirect excitons with $T_X \approx T_{lattice}$: (1) use a separation in time and study the indirect excitons a few nanoseconds after the end of the photoexcitation pulses[10]; (2) use a separation in space and study the indirect excitons beyond the photoexcitation spot. In the second case, excitons can cool down to $T_{lattice}$ as they travel away from the photoexcitation spot.

Here, exploring the spatially and spectrally resolved PL experiments, we have observed a ring structure in the indirect exciton PL and a macroscopically ordered state of indirect excitons appearing in the ring that is farthest from the excitation spot.

At the lowest excitation powers, P_{ex}, the spatial profile of the indirect exciton PL intensity closely follows the laser excitation intensity (Fig. 1a). However, at high P_{ex} we observed a nontrivial pattern for that profile. The pattern is characterized by a ring structure (Fig. 1): the laser excitation spot is surrounded by two concentric bright rings separated by an annular dark intermediate region. The rest of the sample outside the external ring is dark. The internal ring appears near the edge of the laser excitation spot, and the external ring can be more than 100 μm from the excitation spot. Its radius increases with P_{ex}. The ring structure follows the laser excitation spot when it is moved over the whole sample area. This nontrivial spatial profile of the indirect exciton PL intensity is only observed at low temperatures. When the temperature is increased the bright rings wash out, the PL intensity in the inter-ring region and outside the external ring increases, and the profile approaches a monotonic bell-like shape (Fig. 1c).

The external ring is fragmented into circular structures that form a periodic array over macroscopic lengths, up to around 1 mm (Fig. 2a–e). This is demonstrated in Fig. 3e which shows the nearly linear dependence of the fragment positions along the ring versus their number. The fragments follow the external ring either when the excitation spot is moved over the sample area or when the ring

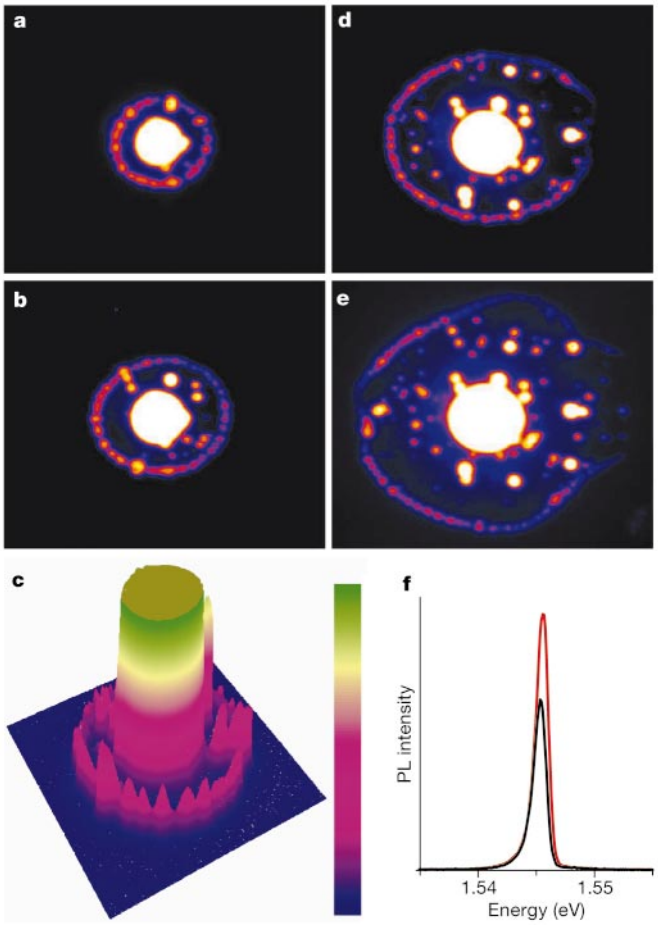

Figure 2 Excitation density dependence of the spatial pattern of the indirect exciton PL intensity. **a**–**e**, The pattern at $T = 1.8$ K, $V_g = 1.22$ V and $P_{ex} = 290$ (**a**), 390 (**b**, **c**), 690 (**d**), and 1,030 (**e**) μW. For **a**, **b**, **d** and **e** the area of view is 530 × 440 μm. The external ring of the indirect exciton PL is fragmented into a periodic chain of circular structures. The fragments follow the external ring both when its radius is changed by varying P_{ex} or when the laser excitation is moved over the sample area. The indirect exciton PL intensity is also strongly enhanced in some spots within the area terminated by the external ring. The position of these spots is fixed on the sample. **f**, Indirect exciton PL spectra in a peak (red) and the adjacent pass (black) on the fragment chain along the ring. Colour bar in **c** starts from zero (blue), and presents a linear scale in arbitrary units.

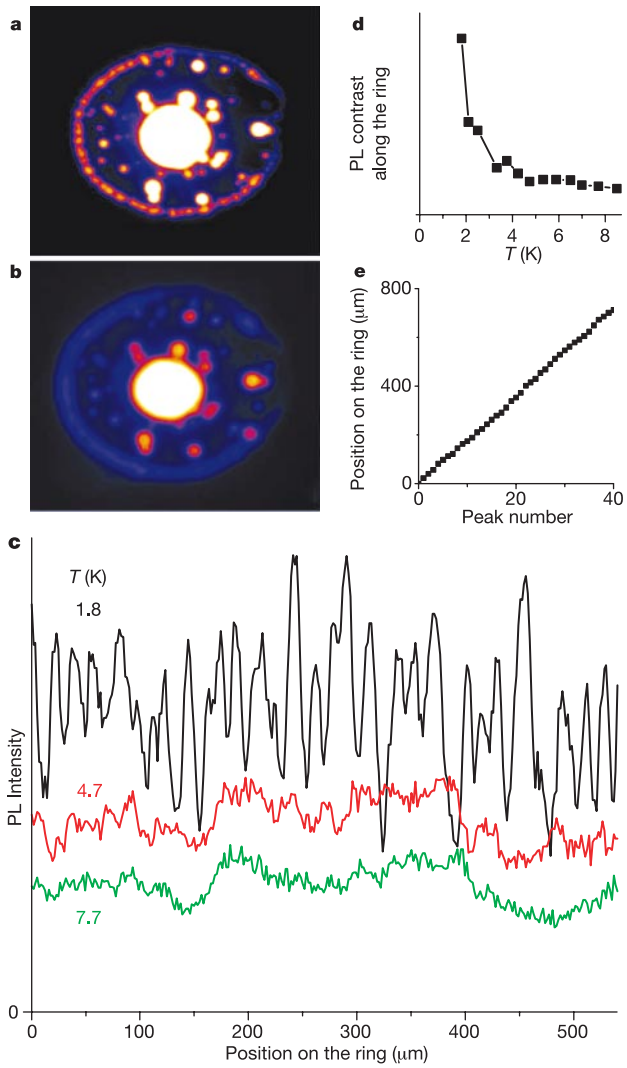

Figure 3 Temperature dependence of the spatial pattern of the indirect exciton PL intensity. **a**, **b**, The pattern at $T = 1.8$ (**a**) and 4.7 K (**b**) for $V_g = 1.22$ V, and $P_{ex} = 690$ μW. The area of view is 475 × 414 μm. **c**, The corresponding variation of the indirect exciton PL intensity along the external ring at $T = 1.8$, 4.7 and 7.7 K. The ring fragmentation into the periodic chain washes out with increasing temperature. This is visualized by the PL contrast (**d**) presented by an amplitude of the Fourier transform. The dependence of the position of the indirect exciton PL intensity peaks along the external ring versus the peak number is nearly linear (**e**), showing that the fragments form a periodic chain.

radius varies with P_{ex}. Along the whole external ring, both in the peaks and the passes, the indirect exciton PL lines are spectrally narrow with the full-width at half-maximum (FWHM) $\approx$ 1.3 meV, considerably smaller than in the centre of the excitation spot; see Figs 2f and 1d. The ring fragmentation is observed at the lowest temperatures only, $T \lesssim 4$ K (Fig. 3a–c). With increasing temperature, the PL contrast along the ring washes out; this is quantified by the amplitude of the Fourier transform of the PL intensity variation along the ring (Fig. 3d).

The spatial pattern shows also that the indirect exciton PL intensity is strongly enhanced in certain fixed spots on the sample; see Fig. 2a–e. We call them localized bright spots (LBS). For any excitation spot location and any P_{ex} the LBS are only observed when they are within the area terminated by the external ring (Fig. 2a–e). In the LBS the indirect exciton PL line is spectrally narrow, the FWHM $\approx$ 1.2 meV, and its energy is locally reduced. The LBS also wash out with increasing temperature.

All these effects are observed on several mesas studied and all experimental data are reproducible after cycling the sample temperature up to room temperature and back to 1.8 K many times. We now discuss the nature of the observed effects.

Under continuous-wave laser excitation a system of photoexcited excitons freely expanding in a QW plane is a thermodynamically open system in a quasiequilibrium. At low densities the indirect excitons are localized by the in-plane potential fluctuations and, therefore, the spatial profile of the indirect exciton PL intensity closely follows the profile of the laser excitation intensity (Fig. 1a). At high densities, however, the repulsive interaction between the indirect excitons screens the in-plane potential fluctuations and, therefore, results in a delocalization of the indirect excitons. Their long lifetime allows them to move far away from the excitation spot before they recombine. As we show below, the lifetime is further enhanced by the exciton motion itself. All these factors facilitate the exciton transport over macroscopic distances up to around 1 mm in our experiments.

For delocalized quasi-two-dimensional excitons only the states inside the radiative zone terminated by the photon cone (Fig. 4a) can recombine radiatively by resonant emission of photons[18]. Those are the states with small in-plane centre of mass momenta $K_{\|} \leq K_0 = E_g\sqrt{\varepsilon}/(\hbar c)$ (E_g is the bandgap and ε is the dielectric constant). The exciton radiative decay rate and thus the exciton PL intensity

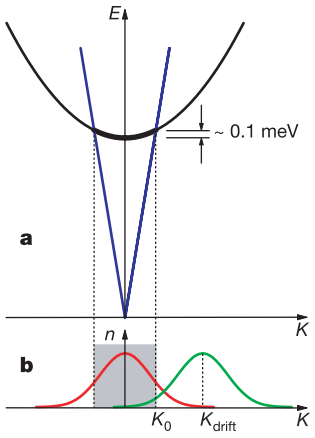

Figure 4 Schematics demonstrating a reduction of emission intensity for excitons in motion. **a**, Energy diagram for the exciton (black) and photon (blue) dispersion, the bold sector of the exciton dispersion indicates the radiative zone. **b**, The schematic momentum distribution of excitons without (red) and with (green) average drift velocity. The exciton radiative decay rate is proportional to the fraction of excitons in the radiative zone (grey area). *E*, energy; *n*, exciton density; K_0, momentum at the radiative zone edge; *K* drift, average drift momentum. See text.

are determined by the fraction of excitons inside the radiative zone. In the centre of the excitation spot the exciton gas is characterized by a high T_X, larger than $T_{lattice}$ (ref. 10). Under continuous-wave photoexcitation, there is a continuous flow of excitons out of the excitation spot owing to the exciton drift and diffusion (other mechanisms such as ballistic transport and phonon wind may also be contributing to the exciton cloud expansion). The exciton diffusion originates directly from the exciton density gradient. The exciton drift also originates from the density gradient as the latter gives rise to the gradient of the indirect exciton potential energy because of the repulsive interaction (see Fig. 1e, f). As the excitons travel away from the excitation spot, T_X decreases with increasing radial distance owing to the energy relaxation of the excitons. The reduction of T_X increases the radiative zone occupation and, therefore, increases the PL intensity; this is seen as the onset of the internal ring. The internal ring is therefore the spatial analogue of the PL jump observed in ref 10. Estimates for the exciton density in the internal ring exceed 3×10^{10} cm^{-2} at the highest P_{ex}, which at $T = 2$ K implies a statistically degenerate Bose gas of indirect excitons (at $n = 3 \times 10^{10}$ cm^{-2} and $T = 2$ K the Bose–Einstein distribution function gives the occupation number of the lowest energy state $\nu = e^{T_0/T} - 1 \approx 0.3$ for the excitons in our coupled QWs where $g = 4$ and $M = 0.21m_0$).

To explain the dark region between the rings we propose the following scenario (Fig. 4). Travelling out of the potential energy 'hill' at the centre of the excitation spot excitons acquire an average drift momentum, K_{drift}. As the height of the potential energy hill at several millielectronvolts (Fig. 1e) is much larger than the kinetic energy at the radiative zone edge ($\hbar^2K_0^2/(2M) \approx 0.1$ meV), K_{drift} can exceed K_0. That means that the moving excitons become optically inactive. This explains the existence of the dark region between the internal and external rings. One aspect of this effect is that the optically inactive excitons move at speeds faster than the speed of sound, $v_s = 3.7 \times 10^5$ cm s^{-1}: even at $K = K_0$, the speed of the excitons is $v = \hbar K_0/M = 1.4 \times 10^6$ cm s^{-1}. Far from the excitation spot the main driving force for exciton transport, the energy gradient, vanishes and the excitons relax down to the lowest energy states. This results in the sharp enhancement of the radiative zone occupation and thus the PL intensity, that is seen as the external ring. We can only give a crude estimate for the exciton density in the external ring: $n \lesssim 10^{10}$ cm^{-2}. As excitons in the external ring relax down to the low momentum states, characterized by low velocities, the exciton flow is stopped and there are almost no excitons outside that ring (Fig. 2a–e).

The most interesting feature of the external ring is its fragmentation into a periodic array. The existence of this periodic ordering shows that the exciton state formed in the external ring has a coherence on a macroscopic length scale. The coherence is not driven by a laser excitation because in our experiment the photoexcited carriers experience many inelastic scatterings before the optically active indirect excitons are formed. Instead, the coherence spontaneously appears in the exciton system. We note that the macroscopic ordering is observed in the same temperature range as bosonic stimulation of exciton scattering[10], below a few kelvin (compare Fig. 3d and Fig. 1f of ref. 10).

The microscopic nature of this ordered exciton state warrants future studies. Comparing with known phenomena, one may suggest that the fragments are vortices in the exciton system and that the ordering is the consequence of a repulsive interaction between the vortices. Within this model, the vortex rotation is continuously supported by the exciton flow out of the excitation spot. Similar to arrays of vortices in atom Bose–Einstein condensates[4], the rotation can be initiated even without an apparent external torque (possibly by a small deviation from axial symmetry of the exciton flow due to the in-plane potential fluctuations, which could cause a branching of the exciton flow, perhaps similar to the branching observed for the electron flow[19]). We also note that a

spontaneous macroscopic flow organization with periodic vortical structures is a general property of thermodynamically open systems, both quantum[1–4] and classical[20], described by nonlinear partial differential equations. A soliton array is another known phenomenon that may be related to the macroscopically ordered exciton state. Multiple solitons ('soliton trains') are known to be stationary solutions of the nonlinear Schrödinger equation on a ring (see ref. 21 and references therein). As the fragmentation that we observe appears abruptly at low temperatures, its nature is probably non-classical.

In-plane potential fluctuations could also influence the position of the fragments on the external ring owing to the pinning effect. However, the pinning effect appears to be small so that fragments remain free to move (for example, with changing of the excitation spot location on the sample) and the deviation of the fragment position out of the periodic array due to the pinning force is also small (Fig. 3e). In contrast, potential fluctuations can play a crucial role in formation of the LBS. We suggest that in the LBS the optically inactive moving indirect excitons are captured by a potential trap formed by in-plane potential fluctuations, relax to the optically active exciton states, and recombine, giving rise to the LBS emission. The LBS will be studied in detail later. In the context of the model discussed here, we note: (1) the existence of LBS in the dark annular region between the two rings confirms the presence of the optically inactive excitons in this region; and (2) the absence of LBS outside of the external ring confirms the absence of excitons there.

The spatial profiles of the direct exciton PL intensity exhibit none of the above effects and almost follow the laser excitation profile for all temperatures and P_{ex} studied; see Fig. 1c (this is also the case for the bulk GaAs emission). This is consistent with a short lifetime of direct excitons that limits the distance they can travel before the recombination and does not allow an effective cooling for them. □

Methods

The $n^+ - i - n^+$ GaAs/AlGaAs coupled QW structure was grown by MBE. The i-region consists of two 8-nm GaAs QWs separated by a 4-nm $Al_{0.33}Ga_{0.67}As$ barrier and surrounded by two 200-nm $Al_{0.33}Ga_{0.67}As$ barrier layers. The electric field in the sample growth direction is monitored by the external gate voltage V_g applied between the highly conducting n^+-layers. For non-zero V_g the ground state is an indirect exciton made of an electron and a hole in different layers (Fig. 1b). The indirect exciton lifetime is in the range of tens and hundreds of nanoseconds. Radiative recombination is the dominant decay mechanism of indirect excitons in our high-quality sample. The indirect exciton energy shift with density, $\delta E(n)$, allows us to evaluate their concentration using $\delta E(n) = 4\pi ne^2 d/\varepsilon$, where d is the effective separation between the electron and hole layers. The sample was excited with a HeNe laser at $\lambda = 632.8$ nm. Spatially resolved PL spectra were detected using a pinhole in the intermediate image plane. In the image experiment, the spatial pattern of the indirect exciton PL intensity was detected by charge-coupled device (CCD) camera using spectral selection of the indirect exciton emission by the interference filter. The spatial resolution was 5 μm.

Received 22 April; accepted 27 June 2002; doi:10.1038/nature00943.

1. Essmann, U. & Träuble, H. The direct observation of individual flux lines in type II superconductors. *Phys. Lett. A* **24,** 526–527 (1967).
2. Yarmchuk, E. J., Gordon, M. J. V. & Packard, R. E. Observation of stationary vortex arrays in rotating superfluid helium. *Phys. Rev. Lett.* **43,** 214–217 (1979).
3. Madison, K. W., Chevy, F., Wohlleben, W. & Dalibard, J. Vortex formation is stirred Bose-Einstein condensate. *Phys. Rev. Lett.* **84,** 806–809 (2000).
4. Abo-Shaeer, J. R., Raman, C., Vogels, J. M. & Ketterle, W. Observation of vortex lattices in Bose-Einstein condensates. *Science* **292,** 476–479 (2001).
5. Keldysh, L. V. & Kozlov, A. N. Collective properties of excitons in semiconductors. *Sov. Phys. JETP* **27,** 521–528 (1968).
6. Lozovik, Yu. E. & Yudson, V. I. A new mechanism for superconductivity: pairing between spatially separated electrons and holes. *Sov. Phys. JETP* **44,** 389–397 (1976).
7. Perakis, I. E. Exciton developments. *Nature* **417,** 33–35 (2002).
8. Fukuzawa, T., Mendez, E. E. & Hong, J. M. Phase transition of an exciton system in GaAs coupled quantum wells. *Phys. Rev. Lett.* **64,** 3066–3069 (1990).
9. Butov, L. V. & Filin, A. I. Anomalous transport and luminescence of indirect excitons in AlAs/GaAs coupled quantum wells as evidence for exciton condensation. *Phys. Rev. B* **58,** 1980–2000 (1998).
10. Butov, L. V. *et al.* Stimulated scattering of indirect excitons in coupled quantum wells: Signature of a degenerate Bose-gas of excitons. *Phys. Rev. Lett.* **86,** 5608–5611 (2001).
11. Butov, L. V., Lai, C. W., Ivanov, A. L., Gossard, A. C. & Chemla, D. S. Towards Bose-Einstein condensation of excitons in potential traps. *Nature* **417,** 47–52 (2002).
12. Larionov, A. V., Timofeev, V. B., Hvam, J. & Soerensen, K. Collective state of interwell excitons in GaAs/AlGaAs double quantum wells under pulse resonance excitation. *JETP Lett.* **75,** 200–204 (2002).
13. Yoshioka, D. & MacDonald, A. H. Double quantum well electron-hole systems in strong magnetic fields. *J. Phys. Soc. Jpn* **59,** 4211–4214 (1990).
14. Zhu, X., Littlewood, P. B., Hybertsen, M. & Rice, T. Exciton condensate in semiconductor quantum well structures. *Phys. Rev. Lett.* **74,** 1633–1636 (1995).
15. Leggett, A. J. Bose-Einstein condensation in the alkali gases: Some fundamental concepts. *Rev. Mod. Phys.* **73,** 307–356 (2001).
16. Popov, V. N. On the theory of the superfluidity of two- and one-dimensional Bose systems. *Theor. Math. Phys.* **11,** 565–573 (1972).
17. Kosterlitz, J. M. & Thouless, D. J. Ordering, metastability and phase transitions in two-dimensional systems. *J. Phys. C* **6,** 1181–1203 (1973).
18. Feldmann, J. *et al.* Linewidth dependence of radiative exciton lifetimes in quantum wells. *Phys. Rev. Lett.* **59,** 2337–2340 (1987).
19. Topinka, M. A. *et al.* Coherent branched flow in a two-dimensional electron gas. *Nature* **410,** 183–186 (2001).
20. Taylor, G. I. Stability of a viscous liquid contained between two rotating cylinders. *Phil. Trans. R. Soc. Lond. A* **223,** 289–343 (1923).
21. Carr, L. D., Clark, C. W. & Reinhardt W. P. Stationary solutions of the one-dimensional nonlinear Schrödinger equation. I. Case of repulsive nonlinearity. *Phys. Rev. A* **62,** 063610-1–063610-10 (2000).

Acknowledgements

We thank A.L. Ivanov for discussions, C.W. Lai and A.V. Mintsev for help in preparing the experiment and K.L. Campman for growing the high quality CQW samples. This work was supported by the Office of Basic Energy Sciences US Department of Energy and by the Russian Foundation for Basic Research (RFBR).

Competing interests statement

The authors declare that they have no competing financial interests.

Correspondence and requests for materials should be addressed to L.V.B. (e-mail: lvbutov@lbl.gov).

Long-range transport in excitonic dark states in coupled quantum wells

D. Snoke*, S. Denev*, Y. Liu*, L. Pfeiffer† & K. West†

** Department of Physics and Astronomy, University of Pittsburgh, 3941 O'Hara Street, Pennsylvania 15260, USA*
† Bell Labs, Lucent Technologies, 700 Mountain Avenue, Murray Hill, New Jersey 07974-0636, USA

During the past ten years, coupled quantum wells have emerged as a promising system for experiments on Bose condensation of excitons, with numerous theoretical[1–6] and experimental[7–12] studies aimed at the demonstration of this effect. One of the issues driving these studies is the possibility of long-range coherent transport of excitons. Excitons in quantum wells typically diffuse only a few micrometres from the spot where they are generated by a laser pulse; their diffusion is limited by their lifetime (typically a few nanoseconds) and by scattering due to disorder in the well structure. Here we report photoluminescence measurements of InGaAs quantum wells and the observation of an effect by which luminescence from excitons appears hundreds of micrometres away from the laser excitation spot. This luminescence appears as a ring around the laser spot; almost none appears in the region between the laser spot and the ring. This implies that the excitons must travel in a dark state until they reach some critical distance, at which they collectively revert to luminescing states. It is unclear whether this effect is related to macroscopic coherence caused by Bose condensation of excitons.

Coupled quantum wells are attractive for Bose condensation of excitons because the lifetime of the excitons can be extended by application of an electric field. A typical band structure is shown in Fig. 1. When electric field is applied normal to the planes of the wells, electrons are confined to one well and holes are confined in